Toxicology Letters 203 (2011) 219–226

Contents lists available at ScienceDirect

Toxicology Letters

journal homepage: www.elsevier.com/locate/toxlet

The disruption of L-carnitine metabolism by aluminum toxicity and oxidative stress promotes dyslipidemia in human astrocytic and hepatic cells

Joseph Lemire, Ryan Mailloux[1], Rami Darwich, Christopher Auger, Vasu D. Appanna*

Department of Chemistry and Biochemistry, Laurentian University, Sudbury, Ontario, Canada, P3E 2C6

ARTICLE INFO

Article history:
Received 21 January 2011
Received in revised form 11 March 2011
Accepted 14 March 2011
Available online 23 March 2011

Keywords:
Aluminum toxicity
Dyslipidemia
Carnitine biosynthesis
Obesity
Neurological disorders

ABSTRACT

L-Carnitine is a critical metabolite indispensable for the metabolism of lipids as it facilitates fatty acid transport into the mitochondrion where β-oxidation occurs. Human astrocytes (CCF-STTG1 cells) and hepatocytes (HepG2 cells) exposed to aluminum (Al) and hydrogen peroxide (H_2O_2), were characterized with lower levels of L-carnitine, diminished β-oxidation, and increased lipid accumulation compared to the controls. γ-Butyrobetainealdehyde dehydrogenase (BADH) and butyrobetaine dioxygenase (BBDOX), two key enzymes mediating the biogenesis of L-carnitine, were sharply reduced during Al and H_2O_2 challenge. Exposure of the Al and H_2O_2-treated cells to α-ketoglutarate (KG), led to the recovery of L-carnitine production with the concomitant reduction in ROS levels. It appears that the channeling of KG to combat oxidative stress results in decreased L-carnitine synthesis, an event that contributes to the dyslipidemia observed during Al and H_2O_2 insults in these mammalian cells. Hence, KG may help alleviate pathological conditions induced by oxidative stress.

1. Introduction

Industrialization, anthropogenic activities, natural phenomena and increased use of man-made chemicals, have triggered a sharp rise in pollutants in our daily life. This situation has led to a devastating impact on human health. Numerous diseases are known to be caused by these environmental toxins (Betarbet et al., 2000; Briggs, 2003; Sherer et al., 2002). While phthalates, chemicals widely utilized in consumer products, disrupt reproductive functions in males, pollutants like polychlorinated benzenes are responsible for various forms of cancers (Foster, 2006; Liu et al., 2010; Swan, 2008). Gaseous pollutants such as CO, NO_2, and SO_2 impair cardiac functions (Rosenlund et al., 2006). Environmental metal contaminants have also been documented to be responsible for a variety of medical conditions. Whereas manganese, a constituent of anti-knock agent induces Parkinson's disease-like disorders, the presence of arsenic in drinking water has been linked to cardiovascular diseases due to its ability to perturb nitric oxide (NO) homeostasis (Bhatnagar, 2006; Guilarte, 2010).

Aluminum (Al), the most widely occurring metal in the earth's crust has become a health threat due to its increased bioavailability in the environment and its presence in consumer goods (Kaizer et al., 2008). This trivalent metal has been associated with Alzheimer's disease, anemia, and osteomalacia (Kaizer et al., 2008). Its ability to mimic iron (Fe), interfere with calcium (Ca) signaling pathways, and bind to phosphate moieties appears to contribute to the toxicity of Al. We have recently demonstrated how Al triggers oxidative stress, disrupts oxidative phosphorylation, and compels HepG2 cells to adopt an anaerobic respiratory regime in an effort to generate ATP, a metabolic switch mediated by the stabilization of hypoxia inducible factor-1α (HIF-1α) (Mailloux and Appanna, 2007). Aconitase (ACN), the gate-keeper to the tricarboxylic acid (TCA) cycle is severely diminished in the presence of Al due to the perturbation of the Fe–S cluster (Mailloux et al., 2006; Middaugh et al., 2005; Zatta et al., 2000). These Al-induced metabolic changes, help to siphon carbohydrates towards lipogenesis turning hepatocytes into fat-producing engines (Mailloux et al., 2007a).

In this report, we have examined the molecular mechanisms responsible for the inability of two mammalian cell lines, namely HepG2 and astrocytoma (CCF-STTG1) to degrade lipids and their propensity to accumulate lipids when challenged by H_2O_2 and Al respectively. L-Carnitine is a non-essential amino acid involved in the transport of fatty acid derived acyl groups into the mitochondria (Muniyappa, 2010). Its synthesis is a multi-step enzymatic process that necessitates the participation of lysine, methionine, and KG. The homeostasis of this biomolecule plays a central role in the metabolism of lipids (Vaz and Wanders, 2002). Here, we demonstrate how Al and H_2O_2 interfere with L-carnitine biosynthesis by impeding two key enzymes mediating the synthesis of this metabolite. The significance of KG metabolism in anti-oxidative defense

* Corresponding author at: 935 Ramsey Lake Rd, Sudbury, Canada. Tel.: +1 705 675 1151x2112; fax: +1 705 675 4844.
E-mail address: vappanna@laurentian.ca (V.D. Appanna).
[1] Present address: Department of Biochemistry, Microbiology and Immunology, Faculty of Medicine, University of Ottawa, 451 Smyth Road, Ottawa, ON, Canada, K1H 8M5. Tel.: +613 562 5800x8217.

0378-4274/$ – see front matter © 2011 Elsevier Ireland Ltd. All rights reserved.
doi:10.1016/j.toxlet.2011.03.019

and L-carnitine biogenesis during Al and H_2O_2 toxicity is discussed. The resulting dyslipidemia and its implications in obesity and neurological disorders are also discussed.

2. Materials and methods

2.1. Culturing and isolating CCF-STTG1 and HepG2 cells

The human astrocytoma cell line (CCF-STTG1) was acquired from the ATCC, Manassas, VA, USA. The usefulness of this cell line is derived from its maintenance of normal astrocytic properties (Mentz et al., 1999). The astrocytic cell line was cultured as described in Lemire et al., 2008. HepG2 cells were a gift from Dr. Templeton (University of Toronto) and were grown as described in Mailloux et al. (2007a,b). It is a commonly utilized model system to study hepatic metabolism (Goya, 2009). Although these are cellular model systems, they do provide valuable information of the molecular workings of the respective organs (Donato et al., 2010; Mentz et al., 1999). When a confluency of 75% was reached, the cell monolayer was washed with Phosphate Buffered Saline [PBS (136 mM sodium chloride, 2.5 mM potassium chloride, 1.83 mM dibasic sodium phosphate, and 0.43 mM monobasic potassium phosphate) pH 7.4]. The astrocytic cells were re-supplemented with serum-free media containing 2.5 mM lactate chelated to varying amounts of Al (0.01–0.1 mM) or 2.5 mM lactate with 40 μM H_2O_2. Cells exposed to lactate (2.5 mM) alone served as the control. HepG2 cells were resupplemented with serum-free media containing 2.5 mM citrate complexed to varying amounts of Al (0.01–0.25 mM) or 2.5 mM citrate with 40 μM H_2O_2. Cells exposed to citrate (2.5 mM) alone served as the control (Mailloux et al., 2007a; Mailloux and Appanna, 2007). To perform recovery experiments, after the 24 h-stressing period, the cells were incubated with serum-free media resupplemented with 5 mM KG or 5 mM carnitine for 8 h. For lipid degradation experiments, HepG2 cells were given 2 mM palmitate complexed to BSA (defatted BSA served as a control) for 24 h following the stressing step. Purity of the fractions was deduced by detecting the levels of VDAC (mitochondria) and (F-actin) cytosol. Protein content was analyzed by the Bradford assay using Bovine Serum Albumin (BSA) as the standard (Bradford, 1976).

2.2. Metabolite analysis

To quantify the cellular levels of succinate, and α-ketoglutarate (KG), cells were treated with 1% perchloric acid and then analyzed by HPLC. Samples were injected into a C_{18}-reverse phase column (Phenomenex) working at a flow rate of 0.7 ml/min. The mobile phase consisted of 20 mM KH_2PO_4 (pH 2.9 with 6 N HCl). Total carnitine was measured by a modified method described in Minkler et al. (2008). Briefly, the soluble cell free extracts were subjected to a 1:4 digestion in 1 M KOH diluted in methanol for 60 min at 50 °C to remove the acyl groups from the carnitine (Minkler et al., 2008). The hydrolyzed carnitine was then injected into a in a C_{18}-reverse phase column (Phenomenex) working at a flow rate of 0.2 ml/min. The mobile phase consisted of 20 mM KH_2PO_4 (pH 7.0 with 6 N HCl) and 20% acetonitrile. Free L-carnitine levels were measured using tandem HPLC analysis. L-Carnitine and its derivatives were separated at a flow rate of 0.7 ml/min, at a retention time of 4 min. The samples were collected and then subsequently reinjected in a C_{18}-reverse phase column (Phenomenex) working at a flow rate of 0.2 ml/min. The mobile phase consisted of 20 mM KH_2PO_4 (pH 2.9 with 6 N HCl) and 20% isopropanol. Palmitate consumption was measured by isolating the cytoplasm by centrifugation at 180,000 × *g* for 2 h to remove any membranes. Following an extraction with hexane, the organic layer was analyzed for palmitate (Schotz et al., 1970). The mobile phase utilized was 95% hexane: 5% isopropanol. Fatty acids were detected at 210 nm. The separated metabolites were compared with known standards, and the metabolite mixtures were spiked with the given metabolites to confirm peak identities.

2.3. Fluorescence microscopy

To visualize ROS formation and lipid accumulation, immunofluorescence microscopy was utilized. CCF-STTG1 or HepG2 cells were grown to a minimal density on coverslips and treated with control, Al, and H_2O_2 conditions as described. The coverslips were washed with 0.5 mM EDTA and PBS and prepared for microscopic examination (Lemire et al., 2008). For the detection of ROS levels within the astrocytes, the cells were incubated with 20 μM of dicholorodihydrofluorescein diacetate (DCFH-DA) in α-MEM and 10% FBS for 1 h at 37°C (Lemire et al., 2009). Lipids and triglycerides were visualized by incubating the cells in Oil Red O (0.5% in PBS) for 10 min at 37°C (Mailloux et al., 2007a). The nucleus was identified using Hoechst 33528 (2.5 μg/ml in PBS). The cells were subsequently examined using an inverted deconvolution microscope (Zeiss, Peabody, MA, USA).

2.4. Blue Native PAGE (BN PAGE) and In-gel activity assays

BN PAGE was performed as described in Mailloux et al. (2007b) and Schagger and von Jagow (1991). Gradient gels (4–16%) were preferentially used for these assays. Briefly, 2 μg of protein equivalent/μl was prepared in blue native buffer [500 mM 6-amino hexanoic acid, 50 mM BisTris (pH7.0), and 1% β-dodecyl-D-maltoside]. For soluble proteins, β-dodecyl-D-maltoside was omitted. Each well of the native gel was loaded with 30 μg of prepared protein samples. Once the electrophoresis was completed, the native gel was incubated in equilibration buffer [25 mM Tris–HCl, 5 mM $MgCl_2$ (pH 7.4)] for 15 min. In-gel activity for ATP-citrate lyase (CL) was monitored by adding 20 mM citrate, 0.75 mM CoA, 0.37 mM ATP, 1.5 mM NADH, 5units/ml malate dehydrogenase (MDH), 16.7 μg/ml dichlorophenolindophenol (DCIP), and iodonitrotetrazolium chloride (INT) (0.5 mg/ml) (Mailloux et al., 2007a). Acetyl-CoA carboxylase (ACC) activity was ascertained by the release of Pi as described in (Simonovic et al., 2004). Briefly, the gel was equilibrated and incubated in 10 mM ATP, 10 mM HCO_3^-, and 1 mM acetyl-CoA for 1 h. The gel was rinsed thrice with ddH_2O followed by 10 min incubation with the phosphate precipitation reagent [$(NH_4)_2MoO_4$ (1.06 g) in 1.37 ml triethylamine and 9.2 ml conc. HNO_3] (Mailloux et al., 2007a). BADH activity was monitored by adding 5 mM γ-butyrobetaine (Sigma), 0.5 mM NADH, 16.7 μg/ml DCIP, and 0.4 mg/ml INT in equilibration buffer. BBDOX activity was ascertained by the addition of 5 mM γ-butyrobetaine, 5 mM α-ketoglutarate, 2.5 mM sodium ascorbate, 0.15 mM ferrous sulfate, and 0.4 mg/ml INT in equilibration buffer. Activity bands were achieved by coupling of INT by ascorbate, a method modified from (May et al., 1995). The reactions were halted using a destaining solution (50% methanol and 10% glacial acetic acid). Negative controls were run routinely with activity stains omitting either substrate or cofactor to ensure band specificity. Bands were quantified using the densitometry suite in the Scion Imaging™ software (Scion Corp. Frederick, MD, USA) (Liu et al., 2009).

2.5. Expression analysis

SDS PAGE and 2D SDS PAGE were performed using the modified method catalogued in (Laemmli, 1970; Lemire et al., 2008). Briefly, cells were sonicated and CFE obtained after centrifugation at 400 × *g* were solubilized in 62.5 mM Tris–HCl (pH 6.8), 2% SDS, and 2% β-mercaptoethanol at 100°C for 5 min and electrophoresed on a 10% isocratic denaturing gel. For 2D analysis of protein levels, activity bands from native gels were precision cut from the gel and incubated in denaturing buffer (1% β-mercaptoethanol, 5% SDS) for 30 min and then loaded vertically into the SDS gel. Electrophoresis was carried out as described above. Proteins were detected using a silver staining kit purchased from Bio-Rad (Chenier et al., 2008). Following electrophoresis, the proteins were blotted on to a nitrocellulose membrane (Li-COR) for immunoblotting. Non-specific binding sites on the membrane were blocked by treatment with 5% non-fat skim milk dissolved in TTBS [20 mM Tris–HCl, 0.8% NaCl, 1% Tween-20 (pH7.6)] for 1 h. Primary antibodies were goat polyclonal to carnitine palmitoyl transferase 1 (CPT1) (Abcam), mouse monoclonal to voltage dependent anion channel (VDAC) (Abcam), mouse monoclonal to BBDOX (Abcam), and a mouse monoclonal to actin (Abcam) and were utilized as recommended by the manufacturers. Secondary antibodies consisted of rabbit anti-goat horseradish peroxidase (HRP) conjugated (Sigma), goat anti-mouse horseradish peroxidase (HRP) conjugated (Sigma) or goat anti-mouse Infrared (IR) 700 (LI-COR) conjugated, donkey anti-mouse IR 680 conjugated (LI-COR), respectively. Detection of the immunoblots was documented via a ChemiDoc XRS system (Bio-Rad Imaging Systems) or using an Odyssey Infrared Imager and accompanying software (LI-COR. Lincoln, NE, USA).

2.6. In-cell immunoblots

In-cell western assays were modified from the Odyssey® Infrared Imaging System protocol document (Li-COR doc# 988-08599). Briefly, CCF-STTG1 cells were seeded in 96-well plates at 1.0×10^6 cells/ml. Following seeding (48 h), the cells were grown to 75% confluency and then stressed as described above. After treatment, the media was removed and the cells were washed thrice with PBS. The cells were then fixed with 37% formaldehyde for 20 min at room temperature. The fixing solution was then removed and the cells were rinsed with 0.1% tween-20 in PBS. Blocking ensued using Odyssey® blocking buffer for 2 h. Primary antibody incubations occurred over a 1 h period with gentle shaking. Mouse monoclonal BBDOX (Abcam), mouse monoclonal to actin (Abcam) were both diluted to a concentration of 1:200 in blocking buffer. Secondary antibodies consisted of donkey anti-mouse IR 680 (LI-COR) diluted to 1:1000. Actin served as a relative control. The infrared signal was detected using an Odyssey® Infrared Imager (LI-COR. Lincoln, NE, USA).

2.7. Statistical analysis

All experiments were performed at least three times and in duplicate. Where appropriate the Student *T* test was utilized to assess significance.

3. Results

3.1. Al and H_2O_2 insult lead to the accumulation of the antioxidant, KG

Following a 24 h treatment with H_2O_2 or Al (a pro-oxidant), the CFE from both the astrocyte and HepG2 cells were found to contain increased levels of KG and succinate when subjected to HPLC analyses (Fig. 1). The latter moiety is known to accumulate due to the non-enzymatic decarboxylation of KG by ROS (Fedotcheva

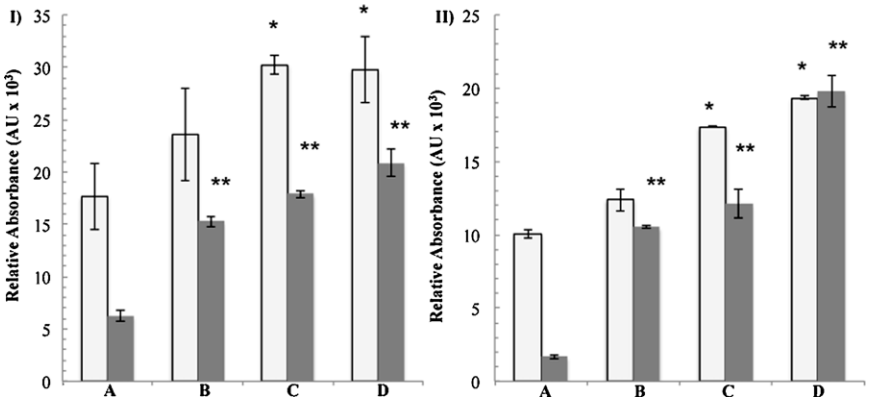

Fig. 1. KG and Succinate levels in astrocytoma and HepG2 cells. CFE was obtained from (I) CCF-STTG1 cells and (II) HepG2 cells treated with (A) Control, (B) 0.01 mM Al, (C) 0.1 mM Al and (D) 40 μM H_2O_2 containing media. HPLC analysis was performed to ascertain □ = KG levels (open bar) and ■ = succinate levels (closed bar) in the CFE. $n = 3 \pm SD$. $P \leq 0.05$ (*indicates a significant change in KG levels, whereas ** is indicative of a significant change in succinate levels).

et al., 2006). We have demonstrated previously that metabolic pathways converge to promote KG production during oxidative stress (Mailloux et al., 2006, 2007b, 2009b). Hence, the activities of KGDH, an enzyme that consumes KG, and NADP-dependent isocitrate dehydrogenase (ICDH-NADP), an enzyme that generates KG, were monitored. Indeed, KGDH activity was diminished while that of ICDH-NADP was enhanced (Fig. 2). KG is a well-characterized anti-oxidant and a number of cell types have been shown to employ this molecule to maintain cellular ROS. The ability of KG to attenuate ROS was confirmed by fluorescence microscopy (Fig. 2). The KG-supplemented cells encouraged a sharp reduction in DCFDA-mediated fluorescence, a fingerprint of ROS. Recovery with 5 mM L-carnitine also reduced ROS levels within the Al-treated cells, however this observation was not as prominent within the H_2O_2 stressed astrocytoma. This may likely be due to the Al-chelating ability of L-carnitine (Gulcin, 2006).

3.2. Al and H_2O_2 treatment disrupt lipid metabolism

We have previously demonstrated that Al treatment induces enhanced lipogenesis in hepatocytes (Mailloux et al., 2007a). Astrocytes and hepatocytes treated with Al and H_2O_2 respectively were characterized with an accumulation of oil droplets within the cells when compared to the controls (Fig. 3). These data clearly indicate that lipid accumulation accompanies Al and H_2O_2 toxicity. These observations were confirmed by measuring the activities of CL and

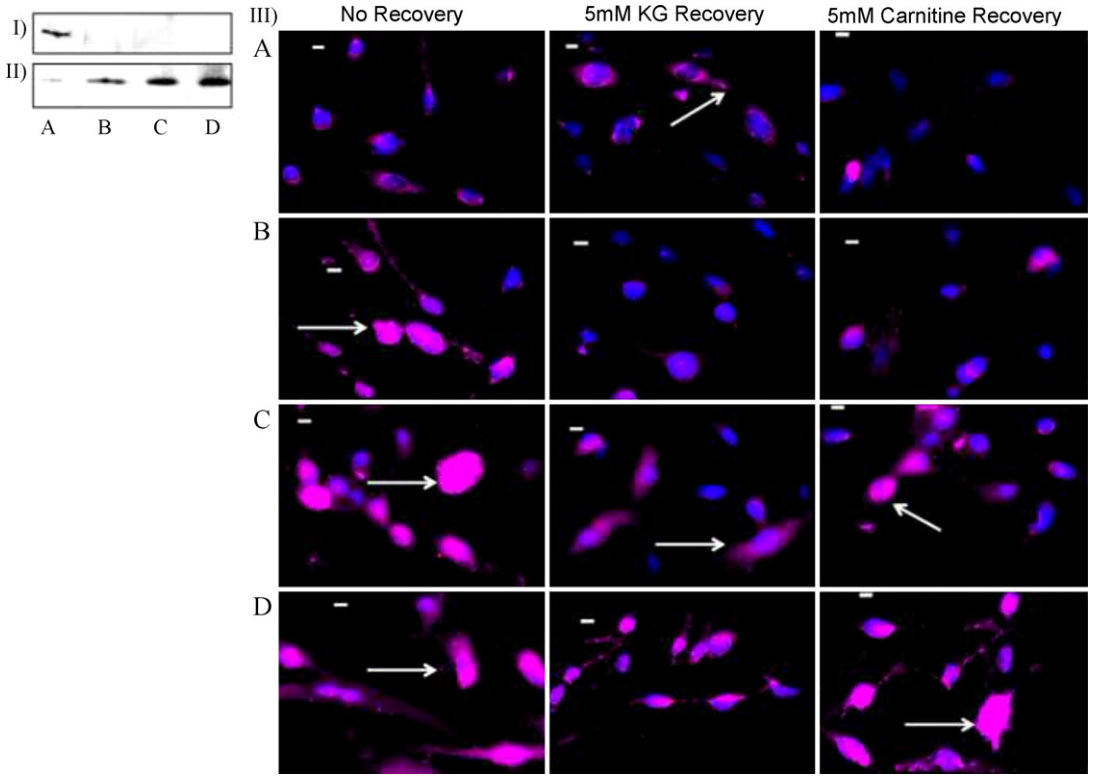

Fig. 2. KG, L-carnitine, and ROS detoxification. Astrocytic cells were analyzed under (A) Control, (B) 0.01 mM Al, (C) 0.1 mM Al and (D) 40 μM H_2O_2 conditions. (I) In-gel activity analysis of mitochondrial CFE for KGDH, (II) In-gel activity analysis of mitochondrial CFE for ICDH-NADP and (III) Fluorescence microscopy was performed at 20X ocular magnification. Blue = Hoechst (nuclei), Purple = DCFDA (ROS). Following a 24 h treatment the cells were recovered with 5 mM KG or 5 mM carnitine for 8 h (note the sharp decrease in ROS). Scale bar = 10 μm. Arrows indicate fluorescence generated by ROS. (For interpretation of the references to colour in this figure legend, the reader is referred to the web version of this article.)

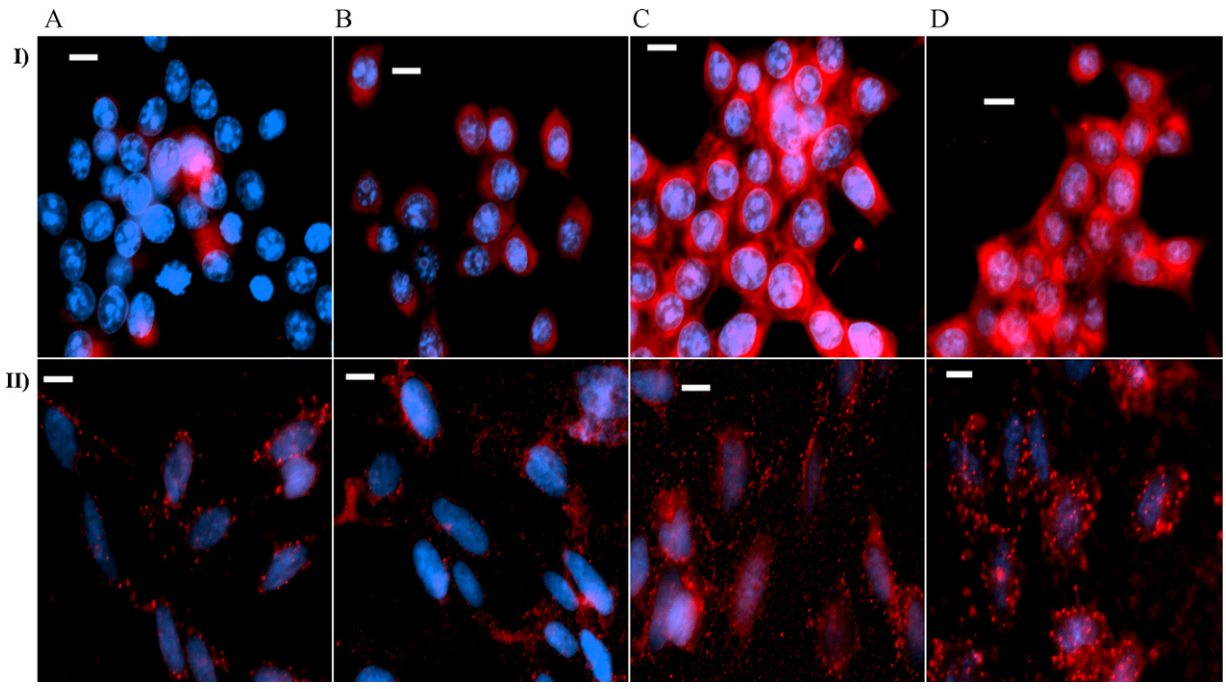

Fig. 3. Lipid accumulation in astrocytic and hepatic cells. Microscopy was performed on (I) astrocytoma cells and (II) HepG2 cells (A) Control, (B) 0.01 mM Al, (C) 0.1 mM Al and (D) 40 μM H_2O_2 treatment at 40X occular magnification. Blue = Hoechst (nuclei), Red = Oil red O (lipids). Scale bar = 10 μm (note the intense red coloration in the stressed cells). (For interpretation of the references to colour in this figure legend, the reader is referred to the web version of this article.)

Table 1
In-gel activity analysis for lipogenic enzymes. The activities of both ACC and CL were ascertained via in-gel activity assay. The bands were subsequently quantified utilizing Scion Imaging™ software, $n = 3 \pm SD$, $P \leq 0.05$.

Enzymes	Astrocytoma			
	Control	0.01 mM A1*	0.01 mM A1*	40 μM H_2O_2*
Citrate lyase acetyl-CoA cacboxylase	337 ± 58 3050 ± 92	1179 ± 112 15870 ± 877	6956 ± 79 16738 ± 1347	9997 ± 207 18646 ± 1739
		HepG2		
		Control	0.25 mM A1*	
Citrate lyase acetyl-CoA cacboxylase		2998 ± 407 10784 ± 780	11306 ± 761 27014 ± 250	

* Indicates a significant difference in enzyme activity.

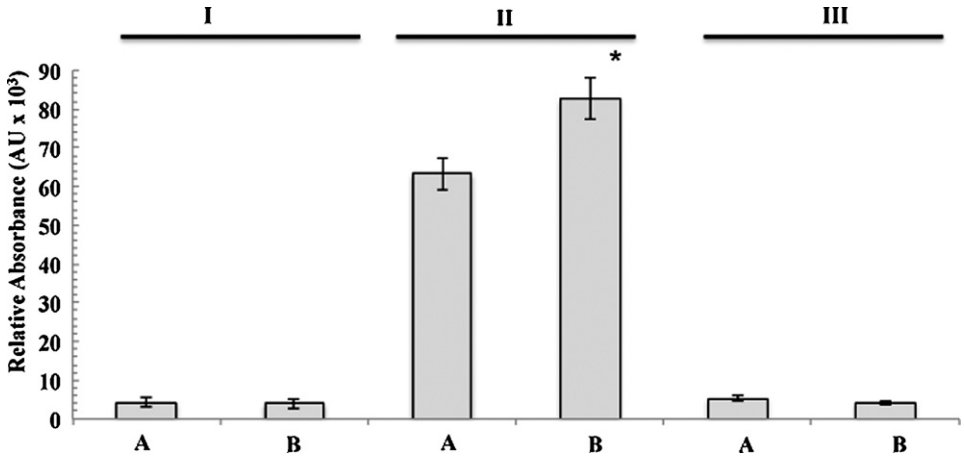

Fig. 4. Palmitate metabolism in Al treated HepG2 cells. Cells were treated with (A) Control and (B) 0.25 mM Al. Following a 24 h treatment period, the cells were subsequently given (I) BSA for 24 h or (II) 2 mM palmitate for 24 h or (III) 2 mM palmitate for 24 h followed by a 5 mM KG recovery for 8 h. HPLC analysis was performed to measure intracellular palmitate. $n = 4 \pm SD$. $P \leq 0.05$ (*indicates a significant lack of consumption of palmitate in the Al stressed conditions).

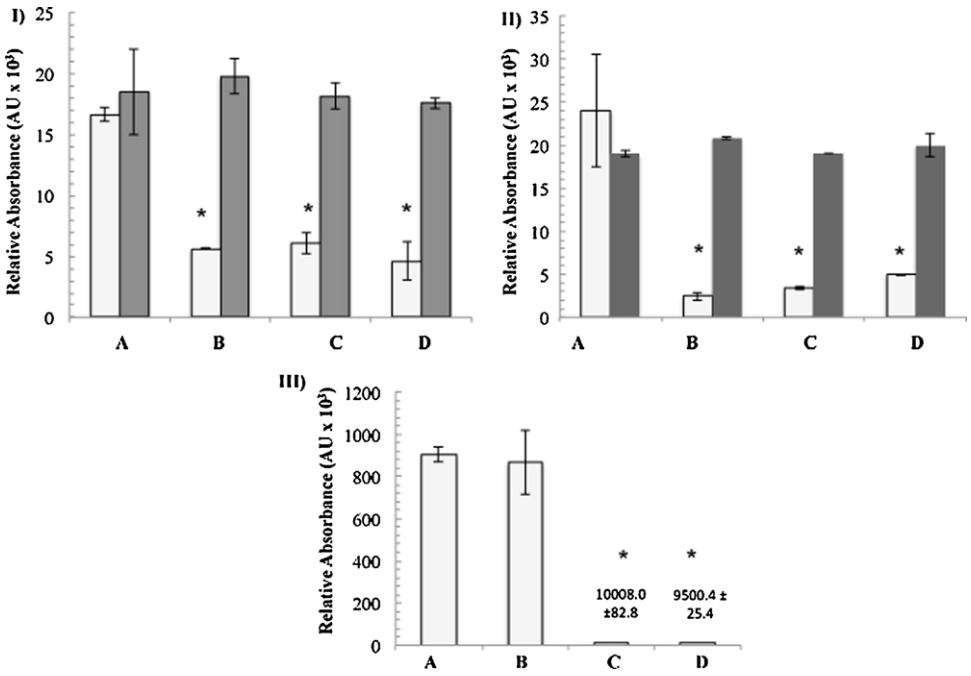

Fig. 5. Carnitine homeostasis in HepG2 and astrocytoma cells. HPLC analysis was done to measure total and free carnitine levels in the CFE from (A) Control, (B) 0.01 mM Al, (C) 0.1 mM Al and (D) 40 μM H_2O_2 treated. (I) free-carnitine levels in astrocytoma cells, (II) free-carnitine levels in HepG2 cells and (III) Total carnitine levels in astrocytoma cells. Where the open bar □ is non-recovered cells and the closed bar ■are cells recovered with 5 mM KG for 8 h. $n = 3 \pm SD$. $P \leq 0.05$ (*indicates a significant change in metabolite levels).

ACC, two key enzymes involved in lipid biosynthesis (Table 1). Both lipid biosynthetic enzymes were markedly increased in the stressed astrocytoma and HepG2 cells. To evaluate the ability of the cells to degrade lipids, the hepatocytes were incubated with 2 mM palmitate for 24 h. HPLC analysis was used to monitor palmitate consumption under different conditions. The Al-stressed cells did not consume the palmitate as readily as the controls (Fig. 4). Furthermore, treatment with 5 mM KG for 8 h resulted in the near complete utilization of palmitate.

3.3. The effects of Al and oxidative stress on L-carnitine homeostasis

To transport lipids into the mitochondria, L-carnitine must be available (Ji et al., 2010). The biogenesis of this metabolite is intricately linked to KG homeostasis, as KG is an essential cofactor for the production of L-carnitine (Vaz and Wanders, 2002). Furthermore, the above data indicate that Al toxicity and oxidative stress (1) perturbs KG homeostasis and (2) induce a metabolic shift that

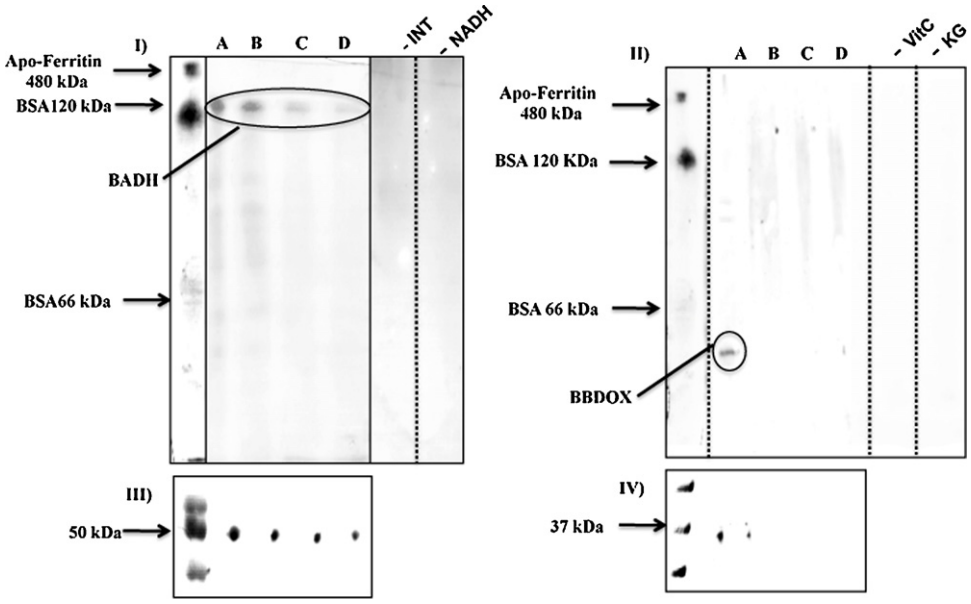

Fig. 6. In-gel activity analysis and expression of enzymes involved in carnitine biosynthesis. astrocytoma cells were treated in (A) Control, (B) 0.01 mM Al, (C) 0.1 mM Al and (D) 40 μM H_2O_2 containing media. (I) In-gel activity analysis of cytoplasmic CFE for BADH (negative controls were performed in the absence of either NADH or INT from the reaction mixture) and (II) In-gel activity analysis of cytoplasmic CFE for BBDOX (negative controls were performed in the absence of either ascorbic acid (VitC) or KG from the reaction mixture). Bands were subsequently precision excised and run on a 10% isocratic SDS–PAGE gel and silver stained for expression analysis of (III) BBADH and (IV) BBDOX.

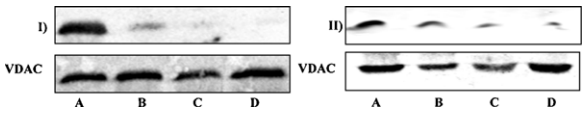

Fig. 7. Expression levels of BBDOX in astrocytoma and HepG2 cells. Immunoblot analysis of CFE for BBDOX was performed in (A) Control, (B) 0.01 mM Al, (C) 0.1 mM Al, and (D) 40 μM H_2O_2 stressed (I) astrocyotma and (II) HepG2 cells. VDAC served as a loading control for these experiments (Note: the cells are least affected by 0.01 mM Al).

favours lipid accumulation. Hence, we reasoned that Al and H_2O_2 treatment might have an influence on L-carnitine metabolism in astrocytoma and HepG2 cells as KG was being utilized in ROS scavenging. Carnitine palmitoyl transferase (CPT 1) is responsible for the transportation of acyl-carnitine from the cytosol to the matrix of the mitochondria (Ji et al., 2010). Immunoblot analysis revealed that the levels of CPT1 was not altered in the Al treated cells (data not included). It is possible that other acyl-carnitine transporters like organic cation/carnitine transporter (OCTN) 2 and the carnitine palmitoyl transporter (CPT) 2, may be affected under Al or ROS insult. However, HPLC analysis of the CFE indicated that free and total L-carnitine levels in both astrocytes and hepatocytes were severely diminished in the Al and H_2O_2 treated cells when compared to the control. It is important to note that in the stressed cells the levels of acylated carnitine were numerous fold lower compared to the control or mildly stressed (0.01 mM Al) cells (Fig. 5).

The diminution of L-carnitine prompted us to probe the activity of two key enzymes involved in L-carnitine biosynthesis, namely BADH and BBDOX, the latter is dependent on KG as a cofactor (Vaz and Wanders, 2002). BN-PAGE analysis revealed that both BADH and BBDOX activities were compromised under Al and H_2O_2 stress (Fig. 6). Following activity analysis, the bands were precision excised and ran on a 10% isocratic SDS PAGE gel, and subsequently silver stained for protein expression analysis. A corresponding decrease in BADH and BBDOX protein levels was observed (Fig. 6). Both enzymes were observed at their approximate predicted molecular masses of 54 kDa and 42 kDa for BADH and BBDOX respectively (Chern and Pietruszko, 1999; Lindstedt and Nordin, 1984). The expression patterns for BBDOX were further confirmed by immunoblot analysis with the aid of an Odyssey infrared imager (Li-COR). The expression of BBDOX, in Al and H_2O_2 stressed astrocytoma and HepG2 cells were diminished compared to the control (Fig. 7). In-cell western blot analysis, followed by quantification with Odyssey infrared imaging software, demonstrated that the expression of BBDOX was markedly lower in the Al and H_2O_2 treated cells compared to the control (Fig. 8).

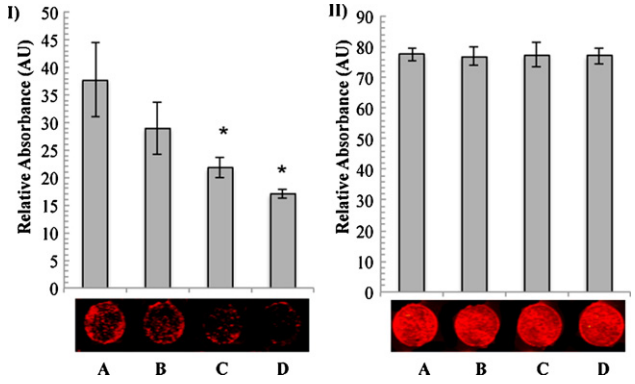

Fig. 8. In-cell immunoblot analysis of BBDOX in astrocytoma cells. Cells were seeded in a 96 well plate and treated with (A) Control, (B) 0.01 mM Al, (C) 0.1 mM Al, and (D) 40 μM H_2O_2. In-cell immunoblots were then performed for (I) BBDOX and (II) Actin. $n = 4 \pm$ SD. $P \leq 0.05$ (*indicates a significant change in BBDOX expression levels).

4. Discussion

In the present investigation, the decrease in L-carnitine levels in the Al and H_2O_2-exposed astrocytoma and HepG2 cells, emerged as an important contributing factor to the dyslipidemia observed in these two mammalian cells. This molecular event appeared to be triggered by the diminished activity and expression of two key enzymes namely BADH and BBDOX, involved in L-carnitine synthesis. Remarkably, this derangement in L-carnitine production was reversed in the presence of KG as were the ROS levels. KG is an essential metabolite in the synthesis of L-carnitine (Vaz et al.,1999, 2001). The depletion of this ketoacid and other necessary cofactors like ascorbic acid, and iron (II) severely impeded the genesis of L-carnitine (a compound generated essentially from lysine and methionine) (Fujita et al., 2009). Due to the oxidative effects of both Al and H_2O_2, cells enhance anti-oxidative defense systems. NADPH-generating enzymes are overexpressed in Al-challenged hepatocytes (Mailloux et al., 2007b, 2009a).

Keto acids are also an excellent source of anti-oxidative power due to their ability to neutralize ROS. While pyruvate neutralizes ROS with concomitant formation of acetate and CO_2, the neutralization of ROS by KG results in the production of succinate and CO_2 (Fedotcheva et al., 2006; Mallet et al., 2002; Tiziani et al., 2009). In the present study, the enhanced production of KG and the elevated levels of succinate in the CFE would point to the utilization of KG in combating the oxidative stress triggered by Al and H_2O_2 stress. Hence, the channeling of KG towards the detoxification of ROS may limit its availability to fuel L-carnitine synthesis and contribute to the inefficacy of the KG-requiring enzymes that mediate the formation of the non-essential branched amino acid. Thus, it is not surprising that enzymes utilizing this cofactor are ineffective in the Al and H_2O_2-challenged cells.

Indeed, the reversal of L-carnitine levels, in the presence of KG would strongly support the notion that this ketoacid is intimately linked with the fate of these enzymes. The involvement of KG in the elimination of ROS has the added benefit of being an important signaling route for anaerobiosis. Succinate, a by-product of the ROS-scavenging function of KG, is a key contributor to the stabilization of HIF-1α. This dicarboxylic acid inhibits prolylhydroxylases (PHD), enzymes effecting the hydroxylation of HIF-1α in a KG-dependent manner (Selak et al., 2005). The hydroxylated HIF-1α is eventually targeted for degradation. However, the utilization of KG in ROS detoxification will ensure elevated levels of succinate and a dearth of KG for the modification of HIF-1α, the conditions will promote anaerobiosis, and is evident during Al and H_2O_2 toxicity (Mailloux et al., 2009a). Additionally, this intracellular environment will favour neither β-oxidation of fatty acids nor the need for L-carnitine, hence the decrease in the synthesis of the latter.

The decrease in L-carnitine levels observed in Al and H_2O_2 – stressed HepG2 and astrocytoma cells may also be due to the ineffective mitochondria promoted by Al and H_2O_2 toxicity. The inability of the mitochondria to perform the TCA cycle and oxidative phosphorylation efficiently will indeed limit the requirement for L-carnitine. Al is an Fe-mimetic. Both Al and H_2O_2 are well known to interfere with Fe-dependent proteins (Chenier et al., 2008). Furthermore, depletion of cellular Fe induces a metabolic phenotype that promotes lipid accumulation in mouse liver (Galy et al., 2010). The mitochondrium is replete with Fe-proteins, hence it is not surprising that this organelle is severely effected by Al and H_2O_2 (Lill and Kispal, 2000). Indeed, ACN an Fe–S cluster containing enzyme is perturbed by Al, as are numerous enzymes of the TCA cycle. Furthermore, oxidative phosphorylation is sharply diminished during Al and H_2O_2 stress. Hence, it is quite likely that the ineffective mitochondria and the decreased levels of L-carnitine evident following Al and H_2O_2-challenge may impede the degradation of palmitate and promote the accumulation of oil droplets (Mailloux

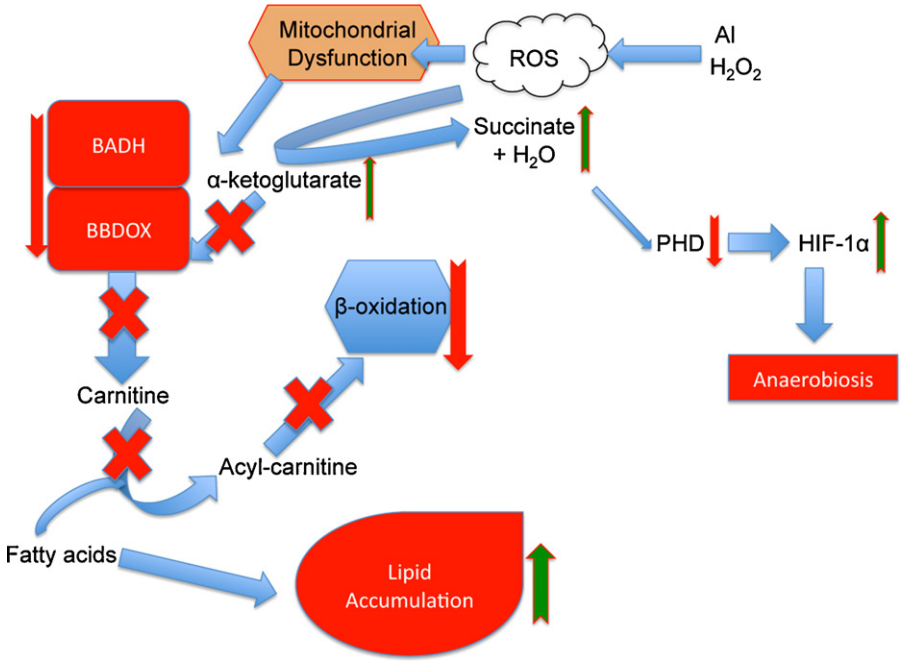

Fig. 9. The effects of Al and H_2O_2 on carnitine metabolism. KG is diverted to ROS detoxification, leading to a perturbation of carnitine synthesis. Fatty acids are directed to lipid storage as β-oxidation can no longer take place. ⇓ = a decrease in levels. ⇑ = an increase in levels. PHD = Prolyl hydroxylase, HIF-1α = Hypoxia inducible factor.

et al., 2006, 2007a). Mitochondrial dysfunction and inhibitors of L-carnitine synthesis are known to promote lipid accumulation and impede fatty acid degradation. Mildronate, a butyrobetaine analogue that has been shown to inhibit L-carnitine synthesis and induces tryglyceride production in mice (Peschechera et al., 2005). Since CPT1 did not change significantly, interference of Al-toxicity with L-carnitine synthesis and mitochondrial Fe-protein might be responsible for the dyslipidemia observed in these cells. However, a negative influence of the oxidative stress and/or Al on other acylcarnitine transporters may not be completely ruled out. It is important to note that supplementation with L-carnitine only partially recovered the Al-stressed cells. This may be attributed to the ability of carnitine to chelate Al and hence mitigate its toxic influence (Gulcin, 2006). Hence, an intricate cross-talk between the mitochondrial status and L-carnitine may exist. As the mitochondria are distressed due to the dearth of the bioavailability of Fe and the oxidative environment triggered during Al and H_2O_2 stress, KG is preferentially earmarked for anti-oxidative defense. This situation would limit the utilization of this essential cofactor in the synthesis of L-carnitine. Thus, mitochondrial dysfunction, oxidative stress, Fe homeostasis, KG levels, and L-carnitine synthesis seem to be intricately linked.

The lack of bioavailable Fe and the increased ROS induced by Al and H_2O_2 render the mitochondria ineffective in performing oxidative phosphorylation. Furthermore, as KG is diverted towards ROS scavenging, L-carnitine biosynthesis is sharply reduced since this keto acid is critical for the genesis of this non-essential amino acid. This cellular environment switches the Al and H_2O_2 stressed cells into fat generating machines as the degradation of fatty acids is inhibited. The release of succinate when KG detoxifies ROS acts as a potent signal for anaerobiosis, a phenomenon common during Al-stress. In conclusion, Al and H_2O_2 toxicity induces mitochondrial dysfunction and leads to the utilization of KG in anti-oxidative defense. As a result, L-carnitine synthesis is diminished; fat accumulation and anaerobiosis are promoted (Fig. 9). It is quite conceivable that these molecular events may contribute to numerous hepatic and neurological diseases triggered by Al and oxidative stress. Hence, KG may provide a therapeutic tool to the pathological conditions evoked by Al and oxidative insults.

Conflict of interest

The authors declare no conflicts of interests.

Acknowledgements

This work was supported by the Northern Ontario Heritage Fund. J.Lemire is a recipient of the Alexander Graham Bell Doctoral Canada Graduate Scholarship.

References

Betarbet, R., Sherer, T.B., MacKenzie, G., Garcia-Osuna, M., Panov, A.V., Greenamyre, J.T., 2000. Chronic systemic pesticide exposure reproduces features of Parkinson's disease. Nat. Neurosci. 3, 1301–1306.
Bhatnagar, A., 2006. Environmental cardiology: studying mechanistic links between pollution and heart disease. Circ. Res. 99, 692–705.
Bradford, M.M., 1976. A rapid and sensitive method for the quantitation of microgram quantities of protein utilizing the principle of protein-dye binding. Anal. Biochem. 72, 248–254.
Briggs, D., 2003. Environmental pollution and the global burden of disease. Br. Med. Bull. 68, 1–24.
Chenier, D., Beriault, R., Mailloux, R., Baquie, M., Abramia, G., Lemire, J., Appanna, V., 2008. Involvement of fumarase C and NADH oxidase in metabolic adaptation of *Pseudomonas fluorescens* cells evoked by aluminum and gallium toxicity. Appl. Environ. Microbiol. 74, 3977–3984.
Chern, M.K., Pietruszko, R., 1999. Evidence for mitochondrial localization of betaine aldehyde dehydrogenase in rat liver: purification, characterization, and comparison with human cytoplasmic E3 isozyme. Biochem. Cell Biol. 77, 179–187.
Donato, M.T., Hallifax, D., Picazo, L., Castell, J.V., Houston, J.B., Gomez-Lechon, M.J., Lahoz, A., 2010. Metabolite formation kinetics and intrinsic clearance of phenacetin, tolbutamide, alprazolam, and midazolam in adenoviral cytochrome P450-transfected HepG2 cells and comparison with hepatocytes and in vivo. Drug Metab. Dispos. 38, 1449–1455.
Fedotcheva, N.I., Sokolov, A.P., Kondrashova, M.N., 2006. Nonezymatic formation of succinate in mitochondria under oxidative stress. Free Radic. Biol. Med. 41, 56–64.
Foster, P.M., 2006. Disruption of reproductive development in male rat offspring following in utero exposure to phthalate esters. Int. J. Androl. 29, 140–147, discussion 181–145.

Fujita, M., Nakanishi, T., Shibue, Y., Kobayashi, D., Moseley, R.H., Shirasaka, Y., Tamai, I., 2009. Hepatic uptake of gamma-butyrobetaine, a precursor of carnitine biosynthesis, in rats. Am. J. Physiol. Gastrointest. Liver Physiol. 297, G681–686.
Galy, B., Ferring-Appel, D., Sauer, S.W., Kaden, S., Lyoumi, S., Puy, H., Kolker, S., Grone, H.J., Hentze, M.W., 2010. Iron regulatory proteins secure mitochondrial iron sufficiency and function. Cell Metab. 12, 194–201.
Goya, L., Martin, M.A., Ramos, S, Mateos, R, Bravo, L, 2009. A cell culture model for the assessment of the chemopreventive potential of dietary compounds. Curr. Nutr. Food Sci. 5, 56–64.
Guilarte, T.R., 2010. Manganese and Parkinson's disease: a critical review and new findings. Environ. Health Perspect. 118, 1071–1080.
Gulcin, I., 2006. Antioxidant and antiradical activities of L-carnitine. Life Sci. 78, 803–811.
Ji, Q., Shi, X., Lin, R., Mao, Y., Zhai, X., Lin, Q., Zhang, J., 2010. Participation of lipid transport and fatty acid metabolism in valproate sodium-induced hepatotoxicity in HepG2 cells. Toxicol. In Vitro 24, 1086–1091.
Kaizer, R.R., Correa, M.C., Gris, L.R., da Rosa, C.S., Bohrer, D., Morsch, V.M., Schetinger, M.R., 2008. Effect of long-term exposure to aluminum on the acetylcholinesterase activity in the central nervous system and erythrocytes. Neurochem. Res. 33, 2294–2301.
Laemmli, U.K., 1970. Cleavage of structural proteins during the assembly of the head of bacteriophage T4. Nature 227, 680–685.
Lemire, J., Mailloux, R.J., Appanna, V.D., 2008. Mitochondrial lactate dehydrogenase is involved in oxidative-energy metabolism in human astrocytoma cells (CCF-STTG1). PLoS ONE 3, e1550.
Lemire, J., Mailloux, R., Puiseux-Dao, S., Appanna, V.D., 2009. Aluminum-induced defective mitochondrial metabolism perturbs cytoskeletal dynamics in human astrocytoma cells. J. Neurosci. Res. 87, 1474–1483.
Lill, R., Kispal, G., 2000. Maturation of cellular Fe–S proteins: an essential function of mitochondria. Trends Biochem. Sci. 25, 352–356.
Lindstedt, S., Nordin, I., 1984. Multiple forms of gamma-butyrobetaine hydroxylase (EC 1.14.11.1). Biochem. J. 223, 119–127.
Liu, X., Liu, M., Zhang, J., Bai, X., Ramos, F., Van Remmen, H., Richardson, A., Liu, F.Y., Dong, L.Q., Liu, F., 2009. Downregulation of Grb2 contributes to the insulin-sensitizing effect of calorie restriction. Am. J. Physiol. Endocrinol. Metab. 296, E1067–1075.
Liu, S., Li, S., Du, Y., 2010. Polychlorinated biphenyls (PCBs) enhance metastatic properties of breast cancer cells by activating Rho-associated kinase (ROCK). PLoS One 5, e11272.
Mailloux, R.J., Appanna, V.D., 2007. Aluminum toxicity triggers the nuclear translocation of HIF-1alpha and promotes anaerobiosis in hepatocytes. Toxicol. In Vitro 21, 16–24.
Mailloux, R.J., Hamel, R., Appanna, V.D., 2006. Aluminum toxicity elicits a dysfunctional TCA cycle and succinate accumulation in hepatocytes. J. Biochem. Mol. Toxicol. 20, 198–208.
Mailloux, R., Lemire, J., Appanna, V., 2007a. Aluminum-induced mitochondrial dysfunction leads to lipid accumulation in human hepatocytes: a link to obesity. Cell Physiol. Biochem. 20, 627–638.
Mailloux, R.J., Beriault, R., Lemire, J., Singh, R., Chenier, D.R., Hamel, R.D., Appanna, V.D., 2007b. The tricarboxylic acid cycle, an ancient metabolic network with a novel twist. PLoS ONE 2, e690.
Mailloux, R.J., Puiseux-Dao, S., Appanna, V.D., 2009a. Alpha-ketoglutarate abrogates the nuclear localization of HIF-1alpha in aluminum-exposed hepatocytes. Biochimie 91, 408–415.
Mailloux, R.J., Singh, R., Brewer, G., Auger, C., Lemire, J., Appanna, V.D., 2009b. Alpha-ketoglutarate dehydrogenase and glutamate dehydrogenase work in tandem to modulate the antioxidant alpha-ketoglutarate during oxidative stress in *Pseudomonas fluorescens*. J. Bacteriol. 191, 3804–3810.
Mallet, R.T., Squires, J.E., Bhatia, S., Sun, J., 2002. Pyruvate restores contractile function and antioxidant defenses of hydrogen peroxide-challenged myocardium. J. Mol. Cell Cardiol. 34, 1173–1184.
May, J.M., Qu, Z.C., Whitesell, R.R., 1995. Ascorbate is the major electron donor for a transmembrane oxidoreductase of human erythrocytes. Biochim. Biophys. Acta 1238, 127–136.
Mentz, S., de Lacalle, S., Baerga-Ortiz, A., Knauer, M.F., Knauer, D.J., Komives, E.A., 1999. Mechanism of thrombin clearance by human astrocytoma cells. J. Neurochem. 72, 980–987.
Middaugh, J., Hamel, R., Jean-Baptiste, G., Beriault, R., Chenier, D., Appanna, V.D., 2005. Aluminum triggers decreased aconitase activity via Fe-S cluster disruption and the overexpression of isocitrate dehydrogenase and isocitrate lyase: a metabolic network mediating cellular survival. J. Biol. Chem. 280, 3159–3165.
Minkler, P.E., Stoll, M.S., Ingalls, S.T., Yang, S., Kerner, J., Hoppel, C.L., 2008. Quantification of carnitine and acylcarnitines in biological matrices by HPLC electrospray ionization-mass spectrometry. Clin. Chem. 54, 1451–1462.
Muniyappa, R., 2010. Oral carnitine therapy and insulin resistance. Hypertension 55, e13.
Peschechera, A., Scalibastri, M., Russo, F., Giarrizzo, M.G., Carminati, P., Giannessi, F., Arduini, A., Ricciolini, R., 2005. Carnitine depletion in rat pups from mothers given mildronate: a model of carnitine deficiency in late fetal and neonatal life. Life Sci. 77, 3078–3091.
Rosenlund, M., Berglind, N., Pershagen, G., Hallqvist, J., Jonson, T., Bellander, T., 2006. Long-term exposure to urban air pollution and myocardial infarction. Epidemiology 17, 383–390.
Schagger, H., von Jagow, G., 1991. Blue native electrophoresis for isolation of membrane protein complexes in enzymatically active form. Anal. Biochem. 199, 223–231.
Schotz, M.C., Garfinkel, A.S., Huebotter, R.J., Stewart, J.E., 1970. A rapid assay for lipoprotein lipase. J. Lipid Res. 11, 68–69.
Selak, M.A., Armour, S.M., MacKenzie, E.D., Boulahbel, H., Watson, D.G., Mansfield, K.D., Pan, Y., Simon, M.C., Thompson, C.B., Gottlieb, E., 2005. Succinate links TCA cycle dysfunction to oncogenesis by inhibiting HIF-alpha prolyl hydroxylase. Cancer Cell 7, 77–85.
Sherer, T.B., Betarbet, R., Greenamyre, J.T., 2002. Environment, mitochondria, and Parkinson's disease. Neuroscientist 8, 192–197.
Simonovic, A.D., Gaddameedhi, S., Anderson, M.D., 2004. In-gel precipitation of enzymatically released phosphate. Anal. Biochem. 334, 312–317.
Swan, S.H., 2008. Environmental phthalate exposure in relation to reproductive outcomes and other health endpoints in humans. Environ. Res. 108, 177–184.
Tiziani, S., Lodi, A., Khanim, F.L., Viant, M.R., Bunce, C.M., Gunther, U.L., 2009. Metabolomic profiling of drug responses in acute myeloid leukaemia cell lines. PLoS One 4, e4251.
Vaz, F.M., Wanders, R.J., 2002. Carnitine biosynthesis in mammals. Biochem. J. 361, 417–429.
Vaz, F.M., van Gool, S., Ofman, R., Wanders, R.J., Ijlst, L., 1999. Carnitine biosynthesis. Purification of gamma-butyrobetaine hydroxylase from rat liver. Adv. Exp. Med. Biol. 466, 117–124.
Vaz, F.M., Ofman, R., Westinga, K., Back, J.W., Wanders, R.J., 2001. Molecular and Biochemical Characterization of Rat epsilon-N-Trimethyllysine Hydroxylase, the First Enzyme of Carnitine Biosynthesis. J. Biol. Chem. 276, 33512–33517.
Zatta, P., Lain, E., Cagnolini, C., 2000. Effects of aluminum on activity of krebs cycle enzymes and glutamate dehydrogenase in rat brain homogenate. Eur. J. Biochem. 267, 3049–3055.